Strong large-scale climate response to North American sulphate aerosols in CESM

Environmental Research Letters

Strong large-scale climate response to North American sulphate aerosols in CESM

To cite this article before publication: Ivonne Mariela García-Martínez *et al* 2020 *Environ. Res. Lett.* in press https://doi.org/10.1088/1748-9326/abbe45

manuscript submitted to *Environmental Research Letters*

Strong large-scale climate response to North American sulphate aerosols in CESM

Ivonne M. García-Martínez [1], Massimo A. Bollasina [1], Sabine Undorf [2]

[1]School of GeoSciences, The University of Edinburgh, Edinburgh, UK
[2]Department of Meteorology and Bolin Centre for Climate Research, Stockholm University, Stockholm, Sweden

Abstract

The effects of increased North American sulphate aerosol emissions on the climate of Mexico and the United States during 1950-1975 are investigated by using two sets of transient coupled experiments with the Community Earth System Model, one with historically evolving emissions, and a second one where North American SO_2 emissions are kept at their pre-industrial levels. The 1950-1975 increase in North American sulphate aerosols is found to have regional and remote impact. Over central U.S. and northern Mexico, the strengthening and westward expansion of the North Atlantic Subtropical High and subsequent intensification of the low-level easterlies, along with local aerosol interactions with radiation and clouds, cause a cooling trend and enhance precipitation. The interaction between the enhanced moisture transport across the Gulf of Mexico and the elevated topography of central Mexico favours positive rainfall on the Atlantic side while suppressing it on the Pacific side. These continental anomalies are embedded in a hemispheric-wide upper-tropospheric teleconnection pattern over the mid-latitudes, extending from the Pacific to the Atlantic basin. Details of the underlying mechanisms –in particular the prominent role of dynamical adjustments– are provided. With SO_2 emissions considerably reduced in the U.S., and the expectation of a continued global decline throughout the 21st century, this study sheds light upon possible ongoing and future regional climate responses to changes in anthropogenic forcing.

1 Introduction

The climate of Mexico and United States (U.S.) has undergone substantial temperature and precipitation changes in the recent decades. For instance, a rapid warming has been identified (Pachauri et al., 2014; Wuebbles et al., 2017), in line with the current global trend. Annual precipitation has decreased over central and southern Mexico, while a positive trend has been observed in northern Mexico and most of the U.S. (Pachauri et al., 2014; Wuebbles et al., 2017). Besides, the intensity and severity of droughts in some regions of the U.S. and Mexico have increased (Stahle et al., 2009; Wuebbles et al., 2017; Vega-Camarena et al., 2018). This has had profound impacts on society, water resources, and the local economy (Stocker et al., 2013, and references therein). Furthermore, CMIP5 models project strong additional warming and a large precipitation reduction over Mexico throughout the 21st century, particularly during the summer, although with considerable uncertainty (Karmalkar et al., 2011; Taylor et al., 2012; Stocker et al., 2013; Colorado-Ruiz et al., 2018). Over the US, temperature is also projected to rise in the coming decades, while precipitation changes are dependent on the location and the season, with a drying trend in most of the U.S. during summer and more precipitation during winter in the northern states (Wuebbles et al., 2017).

Aside greenhouse gases (GHGs), anthropogenic aerosols currently exert a considerable forcing on the Earth's radiative balance (Stocker et al., 2013). In particular, the global radiative forcing from sulphate aerosols during the 20th century is estimated to be of the same

Corresponding author: Ivonne M. García-Martínez, ivonne.garcia@ed.ac.uk

order of magnitude, but of opposite sign, to that of GHGs (Pachauri et al., 2014). Sulphate aerosol emissions have been declining worldwide since the early 1980s and are projected to decrease by up to 80% by the end of the 21st century, leading to an amplification of the GHG-related warming of up to 1°C globally and even more at regional scale (Westervelt et al., 2015). Yet, aerosols represent the largest uncertainty in current estimates of human-driven climate change (Myhre et al., 2014) due to compounding uncertainties associated with model representations of poorly-known aerosol processes, and with the estimation of aerosol emissions.

Anthropogenic aerosols can modify the climate by scattering or absorbing solar radiation, or by changing cloud properties and precipitation processes (e.g., Twomey, 1977; Albrecht, 1989; Charlson et al., 1992; Ming & Ramaswamy, 2009; Boucher et al., 2013, and references therein). Worldwide, aerosols have been found to play a major role in driving the late 20th century weakening of the monsoon over South Asia (Bollasina et al., 2011; Undorf, Polson, et al., 2018), East Asia (Song et al., 2014), and West Africa (Undorf, Polson, et al., 2018), as well as in modulating multidecadal variability in sea surface temperature over the North Atlantic (Booth et al., 2012; Undorf, Bollasina, et al., 2018). Even though North America was one of the largest contributors (along with Europe) to global aerosol emissions, particularly of sulphur dioxide (SO_2, precursor of sulphate aerosols), up to the 1980s (Hoesly et al., 2018), only a few studies have examined the climate response to anthropogenic aerosol variations over this region. Leibensperger et al. (2012) found a cooling of 0.5 to 1°C over the central and eastern U.S. in response to increased U.S. anthropogenic aerosols during 1970-1990. Westervelt et al. (2017) reported a considerable rainfall increase over the central and eastern U.S. and over the North Atlantic associated with the recent SO_2 emissions decline. Yet, the physical mechanisms underlying these changes remain unclear.

The case for North America is particularly relevant as while surface temperature increased worldwide, a cooling trend (the so-called "warming hole"), was observed over the southern U.S. from the early 1950s to the mid 1970s (e.g., Robinson et al., 2002; Wang et al., 2009; Leibensperger et al., 2012). Yet, there is no consensus on the factors driving this muted warming, with some works emphasising the impact of aerosols (Leibensperger et al., 2012; Yu et al., 2014; Mascioli et al., 2017), others the role of internal climate variability (mainly through teleconnections with Pacific sea surface temperatures; Robinson et al., 2002; Wang et al., 2009; Banerjee et al., 2017) or possibly the combined effect of both (Kunkel et al., 2006; Portmann et al., 2009).

A better understanding of the regional as well as large-scale climate response to the 20th century changes in North American aerosol emissions is key to achieve more robust near-future projections in this highly vulnerable region (Karmalkar et al., 2011). In this study, we assess the summertime climate impact of North American anthropogenic sulphate emissions using a state-of-the-art climate model and identify the underpinning mechanisms.

2 Data and Methods

This study makes use of 8-member ensembles of transient coupled experiments with the U.S. National Center for Atmospheric Research (NCAR) Community Earth System Model (CESM) version 1.2.2 (Hurrell et al., 2013). Model setup and experiments are thoroughly described in Undorf, Bollasina, et al. (2018). The atmospheric component is the Community Atmosphere Model (CAM) version 5.3 (Neale et al., 2012), which uses a 3-mode aerosol scheme (MAM3, Ghan et al., 2012) and includes a full prognostic representation of aerosol-cloud interactions (Ghan et al., 2012; Meehl et al., 2013). We analyse an all-forcing ensemble (ALL) driven by time-varying historical emissions from both natural and anthropogenic sources, and a perturbed ensemble identical to ALL but with anthropogenic emissions of sulphate aerosols and sulphur dioxide from North America (continental United States and Canada) fixed at their pre-industrial levels (NoNA). Assuming linearity in the combined responses (which has been shown to be a reasonable approach, e.g.; Polson et al., 2014), the

difference ALL minus NoNA indicates, to a first order approximation, the impact of North American aerosols. Note that non-linear interactions between aerosols and other forcings (such as GHGs and remote aerosols) are removed in the NoNA ensemble, as these only arise when North American aerosols are present. Such an assumption is routinely made in studies investigating the impact of global forcing factors (e.g., Gillett et al., 2016), and more specifically, that of regional aerosol emissions (e.g., Bollasina et al., 2014; Persad & Caldeira, 2018; Undorf, Polson, et al., 2018; Westervelt et al., 2018; Wilcox et al., 2019). We also use several observational datasets to evaluate the present-day model performance: surface temperature from the Climatic Research Unit (CRU) of the University of East Anglia (CRU TS 4.01, at 0.5° resolution, CRU et al., 2017), the Berkeley Global surface temperatures (BEST, at 1° resolution, Rohde et al., 2013), and the GISS Surface Temperature Analysis (GISTEMP, at 2° resolution, Hansen et al., 2010); precipitation from CRU (CRU TS 3.26, at 0.5° resolution, CRU et al., 2019) and from the Global Precipitation Climatology Centre (GPCC v7, at 1° resolution, Becker et al., 2013); and wind fields from the National Centers for Environmental Prediction (NCEP) - NCAR reanalysis (NCEP-NCAR, at 2.5° resolution, Kalnay et al., 1996). A comparison between relevant present-day observed and simulated summer climatology (Text S1 and figure S1) shows that the model can well reproduce magnitude and location of the prominent regional circulation features.

The analysis focuses on summer (June-August), when a large percentage of annual precipitation falls over most of the region (over 60% for southern Mexico and up to 40% for southeast U.S.). The emphasis is on the period 1950-1975, when the cooling trend over the southern U.S.-northern Mexico was the largest (see discussion in section 3). This period encompasses the most pronounced near-linear increase in North American aerosol emissions since pre-industrial times to their peak in the 1970s (figure 1(a); Smith et al., 2011; Hoesly et al., 2018), resulting in a corresponding increase in SO_4 burden (figure 1(b)) and aerosol optical depth (not shown). Temporal changes are identified by least-square linear trends. To detect changes externally forced by anthropogenic aerosols, trends are computed for ensemble mean quantities which allows to largely filter out internal variability. A two-tailed Student's t test is used to assess the significance (at the 95% confidence level) of the difference in the ensemble-mean response between the ALL and NoNA experiments. The extent to which the robustness of the results is affected by internal variability of the climate system is qualitatively estimated by the agreement on the sign of the trends across individual ensemble members.

3 Results

At global scale, the climate response to increased sulphate aerosols features, in accordance with induced changes in the global energy balance, an overall cooling (-0.02°C per decade), particularly strong in the Northern Hemisphere (where aerosol emissions are located; -0.03°C per decade), as well as a global-mean precipitation reduction (-0.003 mm day^{-1} per decade, or about 1% of the model summer climatology) accompanied by a southern shift of the Intertropical Convergence Zone (ITCZ) towards the warmer hemisphere (not shown). This is consistent with previous studies (e.g., Ridley et al., 2015; Allen et al., 2015; Westervelt et al., 2018). At regional scale, the climate response patterns display substantial spatial variability and result from the interplay between thermodynamical and dynamical adjustments to aerosol forcing, as well as local feedback mechanisms.

To place the analysis into context, Figure 1(c)-(d) compares observed and simulated near-surface temperature trends over the southeastern U.S. (black box in figure 2(a)) as a function of the start and end years during the 20th century. A striking feature is the marked 1950-1975 observed cooling trend (figure 1(c), ∼-0.4°C, statistically significant at the 95% confidence level), and the successive warming to present-day. While the largest temperature anomalies are located over the south-central U.S., they are part of a coherent large-scale pattern: the cooling is spatially extensive and spread over the eastern U.S. and northern Mexico, accompanied by a weak warming over the western U.S. (figure 2(a)). This

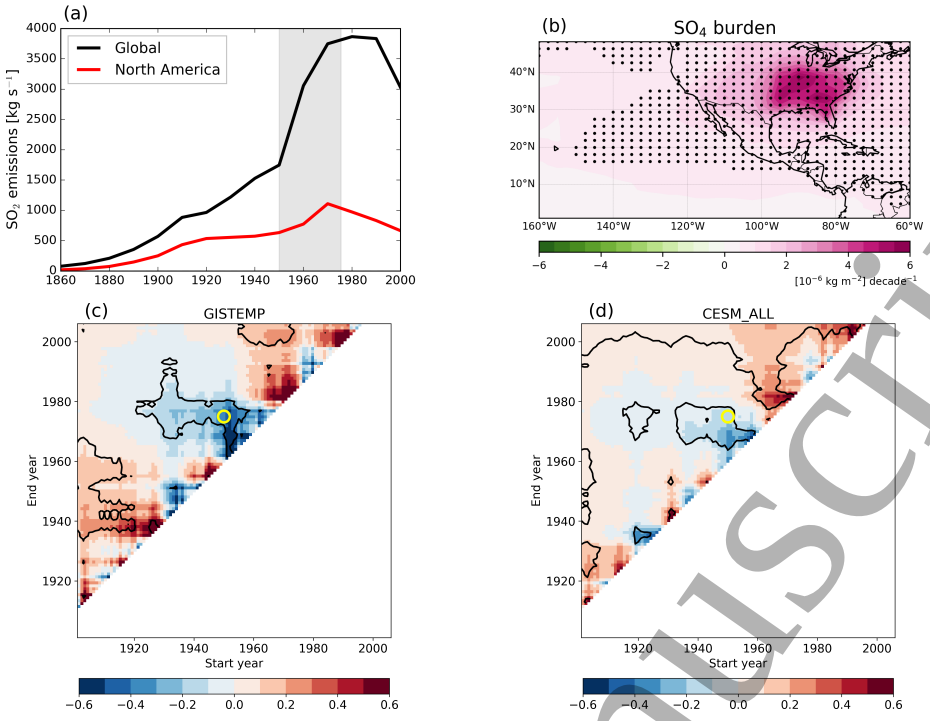

Figure 1. (a) Historical global (black) and North American (red) SO_2 emissions [kg s^{-1}] (data from Lamarque et al., 2010). The period 1950-1975 is shaded in grey. (b) Difference of the 1950-1975 linear trends (ALL minus NoNA) of sulphate burden [(10^{-6} kg m^{-2}) $decade^{-1}$]. Black dots indicate significance at the 95% confidence level. (c) Observed and (d) simulated summer surface temperature trends [°C $decade^{-1}$] for southeast U.S. [80-105°W, 25-35°N, box in figure 2(a)] as a function of the start and end years in the 20th century. Trends over all periods of at least 10 years are plotted. The yellow circle shows the 1950-1975 trend. Significance at the 95% confidence level is denoted by black contours

spatial structure is consistent among various observational datasets (figure 2(b)-(d)) and is in agreement with previous studies (e.g., Leibensperger et al., 2012; Yu et al., 2014; Mascioli et al., 2017). Albeit of weaker magnitude, the CESM_ALL ensemble is able to capture the spatial pattern of the observed 1950-1975 temperature trend reasonably well, in particular the core cooling over the southern U.S. (figures 1(d) and 2(a)-(d)). Notably, the cooling is robust across the 8 ensemble members (figure S3), suggesting it to be primarily due to external forcing. The underestimated magnitude of the cooling in CESM_ALL, however, suggests a potential role of natural variability, or could also be the result of model biases and/or a compensation among different internal coupled processes (e.g., Stevens & Feingold, 2009).

Sulphate aerosols are found to be a key driver of the temperature anomalies described above. The large sulphate burden over the eastern U.S. (Figure 1(b)) results in a significant regional surface cooling (up to -0.5°C per decade, figure 3(a)), enhancing the all-forcing trend and, although weaker, showing a similar spatial pattern to observations (figure 2(a)-(d)). Note that the largest negative temperature trends are located to the west of the region of maximum SO_4 burden and the cooling extends to the Gulf of Mexico and the

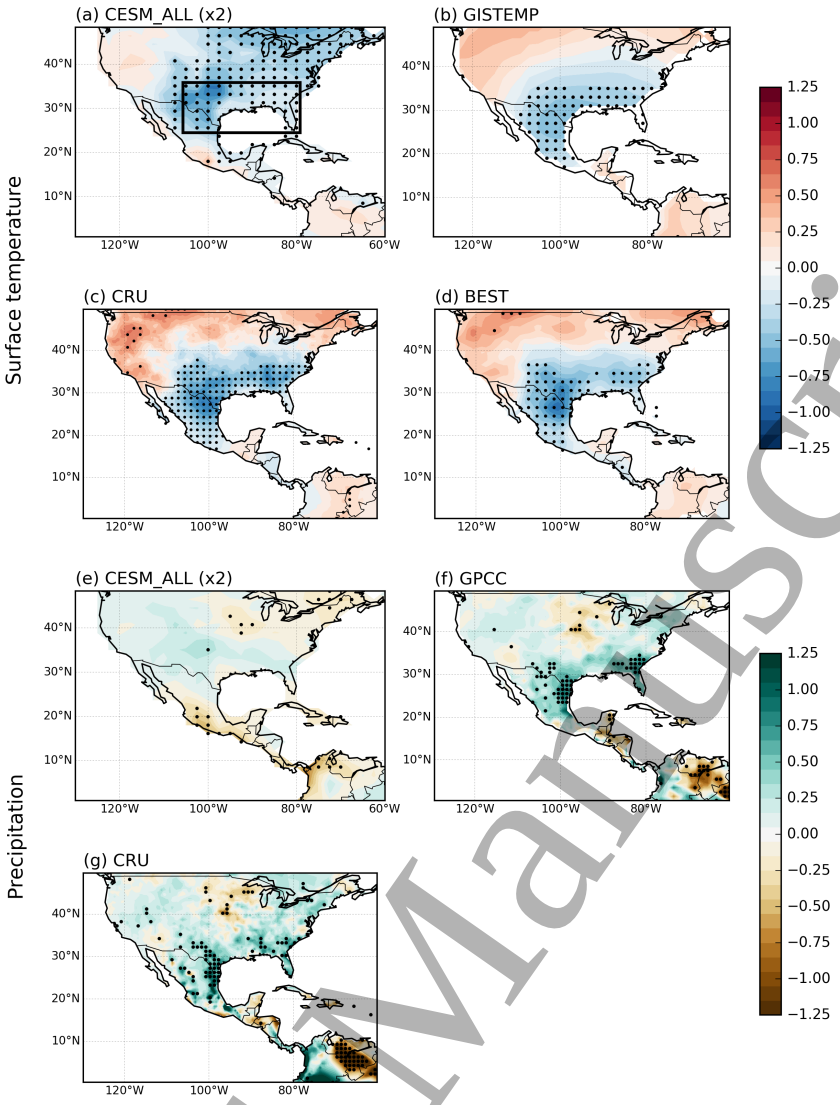

Figure 2. (a)-(d) Simulated and observed 1950-1975 summer surface temperature trends [°C decade^{-1}] for: (a) CESM_ALL, (b) GISTEMP, (c) CRU and (d) BEST. (e)-(f) As (a)-(d) but for precipitation trends [(mm day^{-1}) decade^{-1}] using: (e) CESM_ALL, (f) GPCC and (g) CRU. The significance of the trends at the 95% confidence level is stippled. The CESM_ALL trends in (a) and (e) are multiplied by a factor of 2. The stippling in (c), (d) and (g) has been regridded for clarity

North Atlantic Ocean (figure 3(a)). Furthermore, aerosols appear responsible for the weak warming along the western U.S. and southern Mexico.

The land precipitation response to increased sulphate aerosols (figure 3(b)), while modest over the emission region, features a large-scale wettening of up to 0.15 mm day^{-1} per decade over the Great Plains, the southern U.S. and northern Mexico, accompanied by a significant drying (-0.25 mm day^{-1} per decade) over western Mexico. The aerosol imprint is recognisable in the all-forcing pattern, and the latter is broadly consistent with the observed precipitation trends, although with some regional differences and of weaker magnitude (figure 2(e)-(g)). Over the ocean, widespread drying is found over the western North

Atlantic and the Gulf of Mexico, while a dipole of zonally-elongated anomalies forms over the north-equatorial eastern Pacific (figure 3(b)), suggestive of an aerosol-driven anomalous southwestward shift of the climatological rainfall.

The surface temperature and precipitation changes discussed above are associated with pronounced regional atmospheric circulation anomalies. Changes in the lower-tropospheric atmospheric circulation modulate heat and moisture transport and its convergence over land, an important component of the regional atmospheric water balance (Mo et al., 2005; Nigam & Ruiz-Barradas, 2006; Durán-Quesada et al., 2010; Amador et al., 2016). Additionally, possible variations in the relative contribution of moisture convergence and evaporation may have crucial implications for land water resources and storage under climate change (e.g., Ruiz-Barradas & Nigam, 2006).

The 700-hPa streamfunction (figure 3(c)) shows the development of a low-tropospheric high pressure anomaly over the western North Atlantic with a corresponding pressure decrease towards the subtropical and equatorial Pacific, consistent with a thermodynamical response to the anomalous surface cooling from increased sulphate aerosols and subsequent mass redistribution. However, the centre of the anticyclonic anomaly is not geographically collocated with the largest increase in aerosols over the northeastern U.S. but is displaced northeastward over the Atlantic. This is suggestive of an atmospheric adjustment to aerosol changes, resulting in a large-scale dynamical response pattern extending beyond the source region.

As a result, the North Atlantic Subtropical High (NASH), a key dynamical feature modulating moisture transport towards Mexico and the central-eastern U.S., intensifies, especially on its northern flank, and extends southwestward across central Mexico (figure 3(c)). Anomalous low-tropospheric easterlies blow over the subtropical western Atlantic (figure 3(c)) obstructing the climatological southerlies over the southern U.S. and deflecting the climatological easterlies over the Caribbean southward, which leads to anomalous moisture flux divergence over the eastern seaboard of the U.S. and the northern Gulf of Mexico (figure 3(d)). The interaction between the enhanced easterly moisture transport and the elevated topography of central Mexico favours positive rainfall trends on the Atlantic side, while suppressing rainfall on the Pacific side. A stronger northeastward pressure gradient over the eastern tropical Pacific reinforces the climatological easterlies but also induces anomalous divergence, leading to anomalous drying there and the precipitation shift mentioned above.

The 850-hPa flow associated with the anomalous Atlantic high displays a secondary branch with cyclonic rotation over the eastern U.S. that later joins the flow over the Gulf of Mexico (figure 3(c)). Correspondingly, the anomalous northerly stationary moisture fluxes across the continental U.S. oppose their climatology (e.g., Ruiz-Barradas & Nigam, 2006), and feature divergence over the Great Plains (figure 3(d)). The contribution of this drier northerly flow to the positive precipitation anomaly of the region turns out to be negligible, which suggests a key role of dynamically-induced convergence, rather than transport. Further evidence for this is provided by changes in the 700-hPa circulation (figure 3(c)), the lowest available level above regional topography, which hints to a plausible dynamical link with the moisture convergence pattern via Sverdrup balance and induced vertical motion. We will discuss this link below. The leading role of evaporation anomalies (figure S5) is striking over the southwest U.S. and northern Mexico, a dynamically active region enclosing the northern edge of the North American monsoon, where water recycling is particularly large (evaporation largely exceeds precipitation), and compensates for the regional anomalous vertically-integrated moisture divergence.

An examination of the changes in radiation and clouds sheds light on the realisation of the regional aerosol impact. Increased sulphate loading (figure 1(b)) leads to a marked reduction in all-sky and clear-sky downwelling shortwave radiation at the surface (figure 4(a)-(b)), with decreases of up to -7 and 1.25 W m^{-2} per decade, respectively, over the

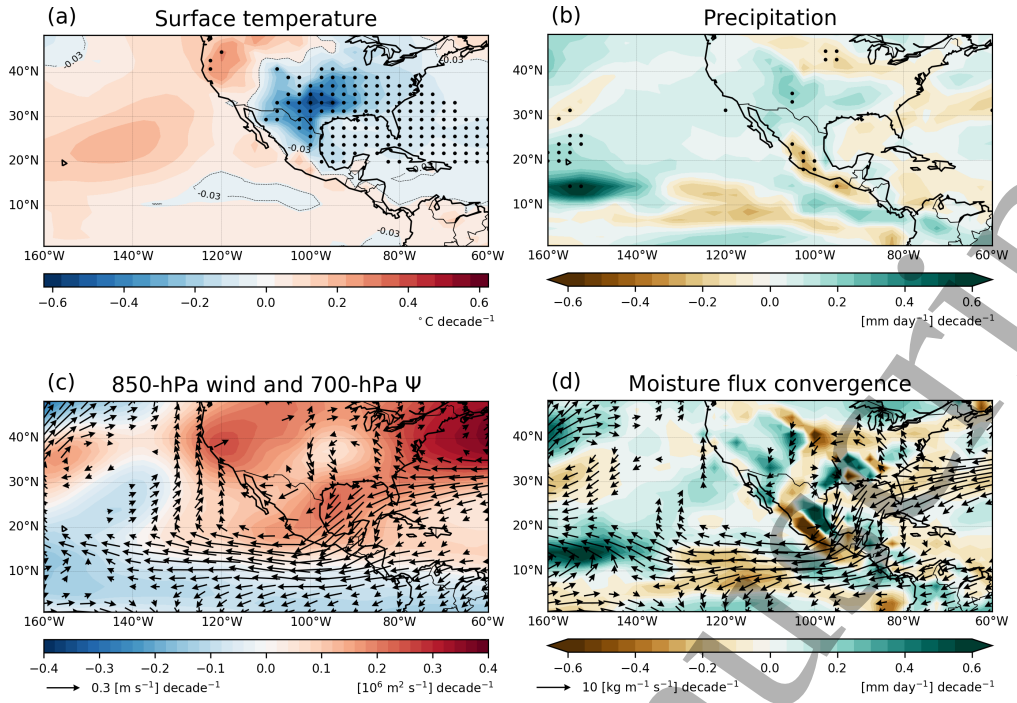

Figure 3. Difference of the 1950-1975 linear trends (ALL minus NoNA) of: (a) surface temperature [°C decade^{-1}], (b) precipitation [(mm day^{-1}) decade^{-1}], (c) 850-hPa wind [vectors, (m s^{-1}) decade $^{-1}$] and 700-hPa streamfunction [ψ, shades, (10^6 m^2 s^{-1}) decade^{-1}], and (d) vertically integrated moisture flux [vectors, (kg m^{-1} s^{-1}) decade^{-1}] and its convergence [shades, (mm day^{-1}) decade^{-1}]. Positive streamfunction values indicate anticyclonic circulation. Significance at the 95% confidence level is stippled, (a)-(b) only. The agreement on the sign of the trends for (a) and (b) across individual ensemble members is shown in figure S4

southeastern U.S. There is also a decrease of -4 W m^{-2} per decade at the top of the atmosphere (TOA, not shown). Shortwave cloud forcing (i.e., the difference between all-sky and clear-sky shortwave radiation) changes are predominant over the aerosol emission region (up to 80% of the all-sky changes), suggesting aerosol-cloud interactions to play a critical role there. Clear-sky shortwave radiation anomalies at the surface and TOA display considerable similarity, reflecting the scattering properties of sulphate aerosols. Over the central and western U.S., both surface and TOA all-sky radiation changes display a decrease while the corresponding clear-sky anomalies are negligible, indicative of increased radiation scattering by more abundant clouds and associated precipitation (figure 3(b)). Similarly, the positive all-sky radiation flux anomalies over western Mexico and further west over the subtropical Pacific are related to drier conditions.

Changes in various cloud characteristics (figure 4(c)-(f)) show similar large-scale response patterns consistent with radiation and precipitation anomalies. Low-level cloud cover (figure 4(c)) features a widespread and significant positive trend over central and eastern U.S. These changes are accompanied by a significant increase in cloud droplet concentration (figure 4(e)) and, although more confined to the east, by a decrease in the droplet effective radius (figure 4(f)), a manifestation of the cloud-albedo effect in the presence of more abundant cloud condensation nuclei and assuming negligible changes in liquid water (Twomey, 1977). However, liquid water path shows a pronounced increase over the eastern U.S. (figure

4(d)), possibly resulting from more abundant droplets held in clouds rather than precipitating out (the cloud-lifetime aerosol effect; Albrecht, 1989) and from an enhanced moistened flux from the Atlantic Ocean. We note that in a large domain of the eastern U.S. there is an increase in the droplet effective radius (excepting the easternmost region mentioned above). A plausible explanation for this is the circulation-driven increase in liquid water path overcompensating for any microphysical-driven decrease in the droplet size. This highlights the complexity of the interplay between cloud microphysics and dynamics in addition to the important role of aerosol-cloud interactions found here. Decreased liquid water path and cloud fraction occur over the north-equatorial Pacific, consistent with the diminished rainfall and enhanced net shortwave radiation at the surface. Anomalies of the opposite sign stretch in a nearly zonal fashion, from the western coast of Central America towards the tropical Pacific, contributing, together with enhanced evaporation (figure S5) by stronger easterlies, to cooling SSTs. The negative SST anomaly is then further spread westward by wind-driven advection. Over the northern Gulf of Mexico, dimming by widespread aerosols leads to cooler SSTs, which locally act to strengthen the anticyclone, as well as, regionally, to enhance the thermal contrast between the Atlantic and Pacific basins and thus the pressure gradient and associated flow.

Given the link between continental surface anomalies and those in the regional circulation, as well as with anomalies over the adjoining oceanic basins (which are known to modulate North American hydroclimate; Burgman & Jang, 2015; Kushnir et al., 2010), it is important to examine the large-scale dynamical context, aiding to an improved mechanistic understanding of how these interactions occur. The pattern of anomalous 500-hPa vertical velocity (not shown) bears a strong resemblance to that of rainfall: wetter (drier) areas generally correspond to ascent (descent), as expected from the approximate balance between diabatic heating and mid-tropospheric vertical motion in the tropics and subtropics. This is clearly discernible over the Pacific and Atlantic oceans, far from land and orographic effects (e.g., across Mexico and the southwestern U.S.). The precipitation excess over the central U.S. and northeastern Mexico is also accompanied by widespread ascent, while an area of strong subsidence is located over the drier northern central U.S.

The 200-hPa geopotential height and meridional wind anomalies (figure 5(a)) further reveal a coherent wave pattern across the Pacific-North American region towards the extratropical Atlantic, indicating that the surface anomalies over the eastern U.S. and Mexico are embedded in a hemispheric-wide upper-tropospheric teleconnection pattern. The equivalent-barotropic nature of the anomalies over North America (with a slight westward tilt with height) is suggestive of a remotely-forced stationary wave response (e.g., Qin & Robinson, 1993). Interestingly, the anomalous height pattern resembles the stationary wave forced by diabatic heating in the central Pacific (Ting, 1994); also the tri-polar pattern across North America bears striking resemblance to the summertime wave pattern associated with variability of the Great Plains low level jet (Weaver & Nigam, 2011) and is further reminiscent of the summer hemispheric-wide wave train identified by Ding and Wang (2005). Insights into the nature of this remote forcing are provided by figures 3(b) and 5; the precipitation anomaly (dipole) over the central Pacific results in vertically-integrated diabatic heating anomalies (up to $+0.16$ K day^{-1} per decade in the positive core, assuming all the heating is due to condensation) and an upper-tropospheric outflow.

Yet, teleconnection patterns are not necessarily generated over the region of the forcing but can be displaced far downstream as determined by the Rossby wave source (RWS; Sardeshmukh & Hoskins, 1988). A wave source dipole coincident with convection anomalies in the central north-equatorial Pacific is clearly recognisable (5(b)-(c)); strong meridional divergent outflow associated with the rainfall anomalies coexist with large meridional vorticity gradients due to the Asian-Pacific jet (e.g., Sardeshmukh & Hoskins, 1988; Qin & Robinson, 1993; Weaver & Nigam, 2008). The RWS distribution features other centres in the extratropics, which can be interpreted as secondary sources generated by the quasi-geostrophic adjustment of the circulation to the wave generated in the primary source region.

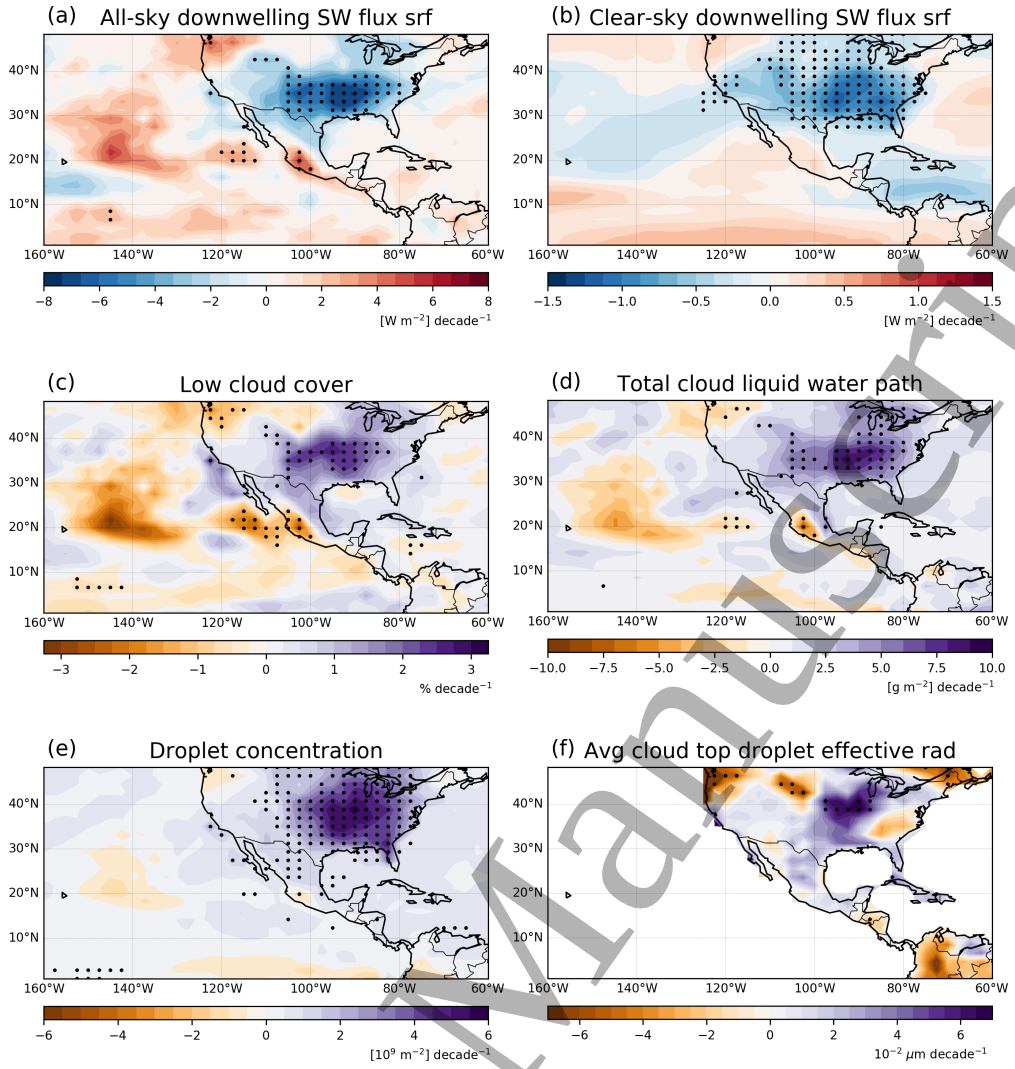

Figure 4. As figure 3 but for: (a) all-sky downwelling shortwave radiation at the surface [(W m^{-2}) $decade^{-1}$], (b) clear-sky downwelling shortwave radiation at the surface [(W m^{-2}) $decade^{-1}$], (c) low cloud cover [% $decade^{-1}$], (d) total cloud liquid water path [(g m^{-2}) $decade^{-1}$], (e) vertically integrated droplet concentration [10^9 m^{-2} $decade^{-1}$], and (f) Average cloud top droplet effective radius [10^{-2} μm $decade^{-1}$]. In (a) and (b), negative values are upward fluxes and indicate cooling. Significance at the 95% confidence level is stippled

The anomalous hemispheric-wide wave pattern identified above, initially instigated by circulation anomalies over the eastern U.S. and of remote central Pacific origin, in turn has an important imprint downstream in modulating the continental aerosol-related signal. In agreement with the Sverdrup vorticity balance (e.g., Rodwell & Hoskins, 2001), strong descent and convection suppression occurs to the east of the upper-tropospheric anomalous ridge and southward flow over the northern Great Plains. Conversely, off the coast of the northeastern U.S., ascent is associated with northward flow on the eastern flank of an anomalous trough. Correspondingly, a dry (wet) anomaly is seen in the precipitation distribution (figure 3(b)). A full mechanistic explanation of the dynamics underlying the formation of the continental precipitation pattern shown in figure 3(b) requires, however, to

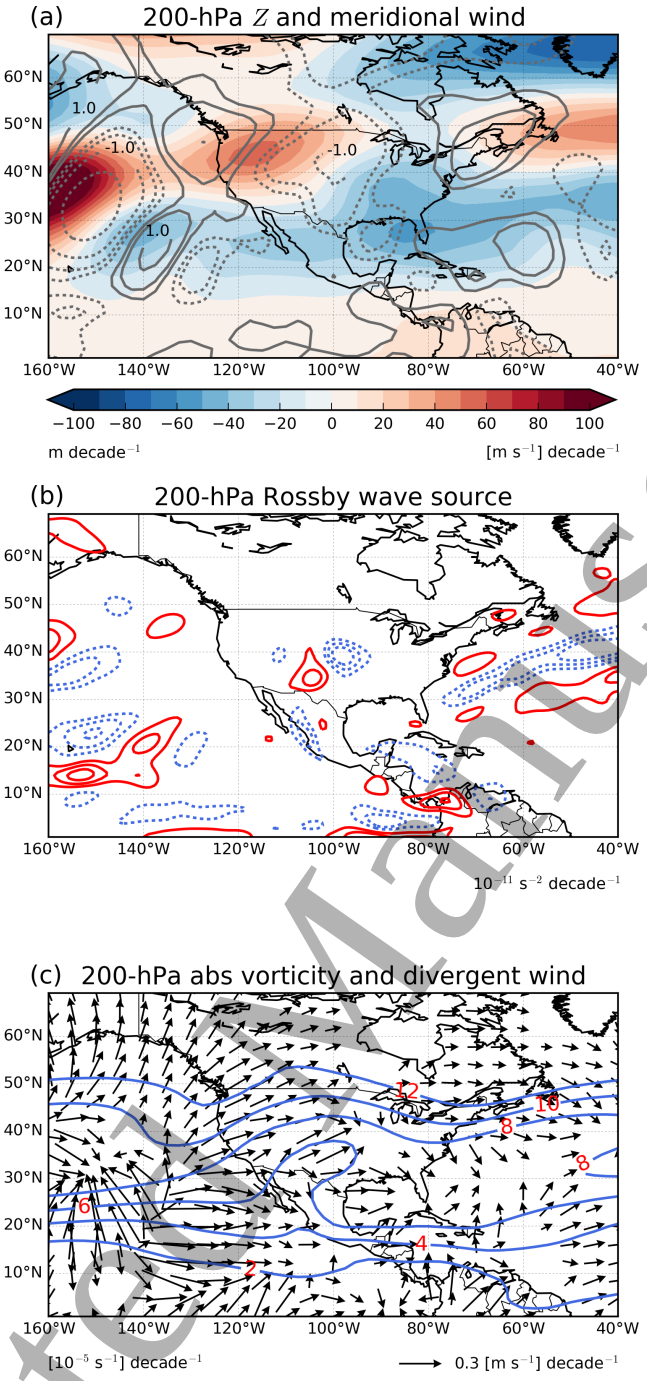

Figure 5. As figure 3 but for the 200-hPa circulation: (a) geopotential height [Z, shades, m decade^{-1}] and meridional wind [grey contours, (m s^{-1}) decade^{-1}], (b) Rossby wave source [10^{-11} s^{-2} decade^{-1}], and (c) absolute vorticity [blue contours, (10^{-5} s^{-1}) decade^{-1}] and divergent wind [vectors, (m s^{-1}) decade^{-1}]. Negative contours are dashed in (a) and (b). The contours shown in (a) are ±0.25, ±0.5, ±1, ±2, and ±3. The contours shown in (b) are ±1, ±2, and ±3

account also for the interaction between upper-tropospheric wave dynamics and the Rockies: anomalous northeasterlies, part of the anomalous upstream anticyclonic circulation, impinge on the western slope of the Rockies (around 30-40°N, 105°W), generating low-tropospheric

convergence and ascent, and thus positive precipitation anomalies. It is also noteworthy that the wave pattern across the eastern U.S., notably the location of the anticyclone over the northern Atlantic, is largely coherent with the near-surface circulation anomalies. Particularly, the low-tropospheric anticyclone over the eastern U.S. is displaced northeastward over the ocean, despite the strong land negative radiative forcing. The surface extension of the upper-level anomalies is thus indicative of an interesting modulation of the aerosol sub-regional imprint by the subsequent large-scale circulation response instigated by induced tropical anomalies.

4 Discussion and Conclusions

This work sought to characterise the summertime climate response to increased North American sulphate aerosols and to understand the underlying mechanisms, particularly the role of atmospheric circulation adjustments –a key factor modulating the conspicuous moisture transport and related hydroclimate over Mexico and the U.S. The focus is on the period 1950-1975, which encompasses the largest increase and subsequent peak in aerosol emissions, and features an anomalous cooling over the eastern U.S. amidst the general continental warming –the "warming hole"–, whose drivers are still the subject of a controversial debate. We used two sets of historical experiments conducted with the CESM model to isolate the impact of regional aerosol changes: a set of all-forcing experiments and an identical one but with North American aerosol emissions kept at their pre-industrial levels.

Regionally, increased aerosols result in widespread large cooling over the central and eastern U.S. and northern Mexico and weak warming over the western U.S. and southern Mexico. Precipitation reduces along the eastern coast of the U.S., opposed to the wetter U.S. continental interior. This is accompanied by a strengthening and westward expansion of the NASH and subsequent intensification of the low-level easterlies and associated moisture transport across the Gulf of Mexico and the eastern north-equatorial Pacific. Both aerosol-radiation and aerosol-cloud interactions contribute to generating these anomalies. At larger scale, a zonal precipitation dipole appears over the eastern tropical Pacific, in contrast with the more meridional and weaker response in the Atlantic sector. The induced anomalous diabatic heating generates a coherent upper-tropospheric signal in the mid-latitudes from the Pacific to the Atlantic basin, which in turn modulates the local aerosol imprint over North America. This emphasises the prominent role of adjustments in the atmospheric circulation and the interplay between local and remote influences in realising the impact of North American aerosols.

One may wonder whether European aerosols, which also increased during the 1950-1975 period by a similar amount, had any influence. Analysis of an additional 8-member all-forcing ensemble with fixed European sulphate aerosol emissions at pre-industrial levels shows that the temperature and precipitation response patterns over Mexico and the U.S. are of smaller magnitude than those driven by North American aerosols (not shown). Aerosols are transported over the subtropical Atlantic basin by the climatological circulation. However, cooling of the underlying SST is minor (-0.03°C per decade), with negligible changes in lower-tropospheric winds. Instead, regional aerosol dimming induces a large anomalous anticyclone over northeastern Europe extending throughout the troposphere, which in turn leads to an upper-tropospheric wave-train propagating across Eurasia (similarly to Undorf, 2019). This reaches the maximum amplitude over Eastern Asia when interacting with the Asian Jet, and then progressively weakens while crossing the eastern Pacific and the U.S.

It is further reasonable to ask whether an aerosol signature is discernible also after the late 1970s, when stringent regulations aimed at improving air quality led to a rapid aerosol decline over the U.S. (halved in the following 30 years, Smith et al., 2011). To ascertain this, we analyse the period 1976-2006. Observations show a warming trend over the whole domain, particularly large over the western U.S., western Mexico, and the northeastern U.S. and southeastern Canada (figure S2(b)-(d)), while the temperature increase is relatively

modest over the central U.S. Also, an overall wettening, with the largest increase over the southeastern U.S. and the Great Plains, is observed (figure S2(f)-(g)). The ALL experiments reproduce the above features well S2(a) and (e). Analysis of the NoNA experiments indicate that aerosols, although decreasing during this period, produce cooling over the central and western U.S., and enhanced precipitation over the southern U.S. and part of the Great Plains. Despite opposite aerosol variations, these anomalous response patterns bear strong resemblance to those during the earlier period, hinting to a common driving mechanism. Support to their dynamically-rooted origin is found in the anomalous rainfall pattern over the Pacific (figure S4): decreased aerosols result in a nearly-uniform northward precipitation shift, with a core over the north-equatorial basin west of 135°W, which generates a wave-like upper-tropospheric response downstream (not shown) similarly to that of the 1950-1975 period. This further emphasises the role of Pacific anomalies as a key factor modulating the aerosol-driven continental anomalies as well as the fundamental contribution of large-scale circulation adjustments.

Although our findings are based on ensemble experiments with 8 members each, the potential role of the internal variability in modulating multi-decadal climate variations over North America cannot be conclusively assessed. In this respect, the use of large ensembles, such as the CESM-LENS (Kay et al., 2015), would help to more robustly isolate the external component in the presence of internally-driven fluctuations.

Furthermore, the results presented here are based on one model only and so they rely on the model's representation of aerosol, cloud, and circulation interactions, which could differ from those in other climate models and/or the real world given the large uncertainties associated with anthropogenic aerosols and their climate interactions. For instance, the aerosol effective radiative forcing (ERF) in CESM1 is known to be large (Zelinka et al., 2014), which could give a stronger climate response to aerosols than that in other climate models. This will depend on how much of the total contribution to the ERF is coming from the processes that drive the regional climate response identified. Despite these limitations, the important role of regional aerosols and their large-scale footprint found here can translate into implications for near-future projections of climate variability over Mexico and the U.S, which affects not just seasonal mean quantities but also climate extremes (see Text S2 and figure S6). With SO_2 emissions considerably reduced in the U.S., and the expectation of a continued global decline throughout the 21st century, this study sheds light upon possible ongoing and future regional climate responses to changes in anthropogenic forcing.

Acknowledgments

IMGM was jointly funded by CONACyT-Mexico and the School of GeoSciences, University of Edinburgh. SU was supported by the European Research Council project (EC-320691) TITAN and the University of Edinburgh. We thank two anonymous reviewers whose comments helped to improve this work. We acknowledge the use of ARCHER, the UK National Supercomputing Service. We thank the CESM project at NCAR. We acknowledge the use of the BEST, CRU, GISTEMP, GPCC, HADEX2 datasets and NCEP-NCAR reanalysis. The data used in this study is available from MAB upon request.

References

Albrecht, B. A. (1989). Aerosols, cloud microphysics, and fractional cloudiness. *Science*, *245*(4923), 1227–1230. doi: https://doi.org/10.1126/science.245.4923.1227

Allen, R. J., Evan, A. T., & Booth, B. B. (2015). Interhemispheric aerosol radiative forcing and tropical precipitation shifts during the late twentieth century. *J. Clim.*, *28*(20), 8219–8246. doi: https://doi.org/10.1175/jcli-d-15-0148.1

Amador, J. A., Durán-Quesada, A., Rivera, E., Mora, G., Sáenz, F., Calderón, B., & Mora, N. (2016). The easternmost tropical Pacific. Part II: Seasonal and intraseasonal modes of atmospheric variability. *Rev. Biol. Trop.*, *64*(Supplement 1), S23–S57. doi:

https://doi.org/10.15517/rbt.v64i1.23409

Banerjee, A., Polvani, L., & Fyfe, J. (2017). The United States "warming hole": Quantifying the forced aerosol response given large internal variability. *Geophys. Res. Lett.*, *44*(4), 1928–1937. doi: https://doi.org/10.1002/2016gl071567

Becker, A., Finger, P., Meyer-Christoffer, A., Rudolf, B., Schamm, K., Schneider, U., & Ziese, M. (2013). A description of the global land-surface precipitation data products of the Global Precipitation Climatology Centre with sample applications including centennial (trend) analysis from 1901–present. *Earth Syst. Sci. Data*, *5*(1), 71–99. doi: https://doi.org/10.5194/essd-5-71-2013

Bollasina, M. A., Ming, Y., & Ramaswamy, V. (2011). Anthropogenic aerosols and the weakening of the South Asian summer monsoon. *Science*, *334*(6055), 502–505. doi: https://doi.org/10.1126/science.1204994

Bollasina, M. A., Ming, Y., Ramaswamy, V., Schwarzkopf, M. D., & Naik, V. (2014). Contribution of local and remote anthropogenic aerosols to the twentieth century weakening of the South Asian Monsoon. *Geophys. Res. Lett.*, *41*(2), 680–687. doi: https://doi.org/10.1002/2013gl058183

Booth, B. B., Dunstone, N. J., Halloran, P. R., Andrews, T., & Bellouin, N. (2012). Aerosols implicated as a prime driver of twentieth-century North Atlantic climate variability. *Nature*, *484*(7393), 228–232. doi: https://doi.org/10.1038/nature11138

Boucher, O., Randall, D., Artaxo, P., Bretherton, C., Feingold, G., Forster, P., ... others (2013). Clouds and aerosols. In *Climate change 2013: the physical science basis. Contribution of Working Group I to the Fifth Assessment Report of the Intergovernmental Panel on Climate Change* (pp. 571–657). Cambridge University Press.

Burgman, R. J., & Jang, Y. (2015). Simulated US drought response to interannual and decadal Pacific SST variability. *J. Clim.*, *28*(12), 4688–4705. doi: https://doi.org/10.1175/JCLI-D-14-00247.1

Charlson, R. J., Schwartz, S., Hales, J., Cess, R. D., Coakley, J. J., Hansen, J., & Hofmann, D. (1992). Climate forcing by anthropogenic aerosols. *Science*, *255*(5043), 423–430. doi: https://doi.org/10.1126/science.255.5043.423

Colorado-Ruiz, G., Cavazos, T., Salinas, J. A., De Grau, P., & Ayala, R. (2018). Climate change projections from coupled model intercomparison project phase 5 multi-model weighted ensembles for mexico, the north american monsoon, and the mid-summer drought region. *Int. J. Climatol.*, *38*(15), 5699–5716. doi: https://doi.org/10.1002/joc.5773

CRU, Harris, I. C., & Jones, P. D. (2017). *CRU TS4.01: Climatic Research Unit (CRU) Time-Series (TS) version 4.01 of high-resolution gridded data of month-by-month variation in climate (jan. 1901- dec. 2016).* Centre for Environmental Data Analysis (CEDA). Retrieved from `https://catalogue.ceda.ac.uk/uuid/58a8802721c94c66ae45c3baa4d814d0` doi: 10.5285/58A8802721C94C66AE45C3BAA4D814D0

CRU, Jones, P. D., & Harris, I. C. (2019). *Climatic Research Unit: Time-series datasets of variations in climate with variations in other phenomena v3.0-v3.26.* Centre for Environmental Data Analysis (CEDA). Retrieved from `https://catalogue.ceda.ac.uk/uuid/3f8944800cc48e1cbc29a5ee12d8542d`

Ding, Q., & Wang, B. (2005). Circumglobal teleconnection in the Northern Hemisphere summer. *J. Clim.*, *18*(17), 3483–3505. doi: https://doi.org/10.1175/JCLI3473.1

Durán-Quesada, A., Gimeno, L., Amador, J., & Nieto, R. (2010). A Lagrangian approach to moisture sources for Central America: Part I. Moisture sources identification. *J. Geophys. Res.*, *15*. doi: https://doi.org/10.1029/2010JD014168

Ghan, S. J., Liu, X., Easter, R. C., Zaveri, R., Rasch, P. J., Yoon, J.-H., & Eaton, B. (2012). Toward a minimal representation of aerosols in climate models: Comparative decomposition of aerosol direct, semidirect, and indirect radiative forcing. *J. Clim.*, *25*(19), 6461–6476. doi: https://doi.org/10.1175/jcli-d-11-00650.1

Gillett, N. P., Shiogama, H., Funke, B., Hegerl, G., Knutti, R., Matthes, K., ... Tebaldi, C. (2016). Detection and attribution model intercomparison project (damip). *Geosci.*

Model Dev., *9*(10), 3685–3697. doi: https://doi.org/10.5194/gmd-2016-74-rc2

Hansen, J., Ruedy, R., Sato, M., & Lo, K. (2010). Global surface temperature change. *Reviews of Geophysics*, *48*(4). doi: https://doi.org/10.1029/2010RG000345

Hoesly, R. M., Smith, S. J., Feng, L., Klimont, Z., Janssens-Maenhout, G., Pitkanen, T., ... others (2018). Historical (1750–2014) anthropogenic emissions of reactive gases and aerosols from the Community Emissions Data System (CEDS). *Geosci. Model Dev.*, *11*(PNNL-SA-123932). doi: https://doi.org/10.5194/gmd-11-369-2018

Hurrell, J. W., Holland, M. M., Gent, P. R., Ghan, S., Kay, J. E., Kushner, P. J., ... others (2013). The Community Earth System Model: a framework for collaborative research. *Bull. Amer. Meteor. Soc.*, *94*(9), 1339–1360. doi: https://doi.org/10.1175/BAMS-D-12-00121.1

Kalnay, E., Kanamitsu, M., Kistler, R., Collins, W., Deaven, D., Gandin, L., ... others (1996). The NCEP/NCAR 40-year reanalysis project. *Bull. Amer. Meteor. Soc.*, *77*(3), 437–472. doi: https://doi.org/10.1175/1520-0477(1996)077⟨0437:TNYRP⟩2.0.CO;2

Karmalkar, A. V., Bradley, R. S., & Diaz, H. F. (2011). Climate change in Central America and Mexico: regional climate model validation and climate change projections. *Clim. Dyn.*, *37*(3-4), 605. doi: https://doi.org/10.1007/s00382-011-1099-9

Kay, J. E., Deser, C., Phillips, A., Mai, A., Hannay, C., Strand, G., ... others (2015). The Community Earth System Model (CESM) large ensemble project: A community resource for studying climate change in the presence of internal climate variability. *Bull. Amer. Meteor. Soc.*, *96*(8), 1333–1349. doi: https://doi.org/10.1175/BAMS-D-13-00255.1

Kunkel, K. E., Liang, X.-Z., Zhu, J., & Lin, Y. (2006). Can CGCMs simulate the twentieth-century "warming hole" in the central United States? *J. Clim.*, *19*(17), 4137–4153. doi: https://doi.org/10.1175/jcli3848.1

Kushnir, Y., Seager, R., Ting, M., Naik, N., & Nakamura, J. (2010). Mechanisms of tropical Atlantic SST influence on North American precipitation variability. *J. Clim.*, *23*(21), 5610–5628. doi: https://doi.org/10.1175/2010JCLI3172.1

Lamarque, J.-F., Bond, T. C., Eyring, V., Granier, C., Heil, A., Klimont, Z., ... others (2010). Historical (1850–2000) gridded anthropogenic and biomass burning emissions of reactive gases and aerosols: methodology and application. *Atmos. Chem. Phys.*, *10*(15), 7017–7039. doi: https://doi.org/10.5194/acp-10-7017-2010

Leibensperger, E., Mickley, L. J., Jacob, D. J., Chen, W.-T., Seinfeld, J., Nenes, A., ... Rind, D. (2012). Climatic effects of 1950–2050 changes in US anthropogenic aerosols–Part 2: Climate response. *Atmos. Chem. Phys.*, *12*(7), 3349–3362. doi: https://doi.org/10.5194/acpd-11-24127-2011

Mascioli, N. R., Previdi, M., Fiore, A. M., & Ting, M. (2017). Timing and seasonality of the United States 'warming hole'. *Environmental Research Letters*, *12*(3), 034008. doi: https://doi.org/10.1088/1748-9326/aa5ef4

Meehl, G. A., Washington, W. M., Arblaster, J. M., Hu, A., Teng, H., Kay, J. E., ... Strand, W. G. (2013). Climate change projections in CESM1 (CAM5) compared to CCSM4. *J. Clim.*, *26*(17), 6287–6308. doi: https://doi.org/10.1175/JCLI-D-12-00572.1

Ming, Y., & Ramaswamy, V. (2009). Nonlinear climate and hydrological responses to aerosol effects. *J. Clim.*, *22*(6), 1329–1339. doi: https://doi.org/10.1175/2008jcli2362.1

Mo, K. C., Chelliah, M., Carrera, M. L., Higgins, R. W., & Ebisuzaki, W. (2005). Atmospheric moisture transport over the United States and Mexico as evaluated in the NCEP regional reanalysis. *J. Hydrometeorol.*, *6*(5), 710–728. doi: https://doi.org/10.1175/JHM452.1

Myhre, G., Shindell, D., & Pongratz, J. (2014). Anthropogenic and natural radiative forcing.
doi: https://doi.org/10.1017/cbo9781107415324.019

Neale, R. B., Gettelman, A., Park, S., Chen, C.-C., Lauritzen, P. H., Williamson, D. L., et al. (2012). Description of the NCAR community atmosphere model (CAM 5.0). *NCAR Technical note*. doi: https://doi.org/10.5065/D6N877R0

Nigam, S., & Ruiz-Barradas, A. (2006). Seasonal hydroclimate variability over North America in global and regional reanalyses and AMIP simulations: Varied representation. *J. Clim.*, *19*(5), 815–837. doi: https://doi.org/10.1175/JCLI3635.1

Pachauri, R. K., Allen, M. R., Barros, V. R., Broome, J., Cramer, W., Christ, R., ... et al. (2014). *Climate change 2014: synthesis report. Contribution of Working Groups I, II and III to the fifth assessment report of the Intergovernmental Panel on Climate Change*. IPCC.

Persad, G. G., & Caldeira, K. (2018). Divergent global-scale temperature effects from identical aerosols emitted in different regions. *Nat. Commun.*, *9*(1), 1–9. doi: https://doi.org/10.1038/s41467-018-05838-6

Polson, D., Bollasina, M., Hegerl, G. C., & Wilcox, L. (2014). Decreased monsoon precipitation in the northern hemisphere due to anthropogenic aerosols. *Geophys. Res. Lett.*, *41*(16), 6023–6029.

Portmann, R. W., Solomon, S., & Hegerl, G. C. (2009). Spatial and seasonal patterns in climate change, temperatures, and precipitation across the United States. *Proc. Natl. Acad. Sci.*, *106*(18), 7324–7329. doi: https://doi.org/10.1073/pnas.0808533106

Qin, J., & Robinson, W. A. (1993). On the Rossby wave source and the steady linear response to tropical forcing. *J. Atmos. Sci.*, *50*(12), 1819–1823. doi: https://doi.org/10.1175/1520-0469(1993)050⟨1819:OTRWSA⟩2.0.CO;2

Ridley, H. E., Asmerom, Y., Baldini, J. U., Breitenbach, S. F., Aquino, V. V., Prufer, K. M., ... others (2015). Aerosol forcing of the position of the intertropical convergence zone since AD 1550. *Nat. Geosci.*, *8*(3), 195. doi: https://doi.org/10.1038/ngeo2353

Robinson, W. A., Reudy, R., & Hansen, J. E. (2002). General circulation model simulations of recent cooling in the east-central United States. *J. Geophys. Res. Atmos.*, *107*(D24), ACL–4. doi: https://doi.org/10.1029/2001jd001577

Rodwell, M. J., & Hoskins, B. J. (2001). Subtropical anticyclones and summer monsoons. *J. Clim.*, *14*(15), 3192–3211. doi: https://doi.org/10.1175/1520-0442(2001)014⟨3192:SAASM⟩2.0.CO;2

Rohde, R., Muller, R., Jacobsen, R., Muller, E., Perlmutter, S., Rosenfeld, A., ... Wickham, C. (2013). A new estimate of the average Earth surface land temperature spanning 1753 to 2011. *Geoinfor. Geostat.: An Overview*, *7*, 2. doi: https://doi.org/10.4172/2327-4581.1000101

Ruiz-Barradas, A., & Nigam, S. (2006). IPCC's twentieth-century climate simulations: Varied representations of North American hydroclimate variability. *J. Clim.*, *19*(16), 4041–4058. doi: https://doi.org/10.1175/JCLI3809.1

Sardeshmukh, P. D., & Hoskins, B. J. (1988). The generation of global rotational flow by steady idealized tropical divergence. *J. Atmos. Sci.*, *45*(7), 1228–1251. doi: https://doi.org/10.1175/1520-0469(1988)045⟨1228:TGOGRF⟩2.0.CO;2

Smith, S. J., van Aardenne, J., Klimont, Z., Andres, R. J., Volke, A., & Delgado Arias, S. (2011). Anthropogenic sulfur dioxide emissions: 1850-2005. *Atmos. Chem. Phys.*, *11*(3), 1101–1116. doi: https://doi.org/10.5194/acp-11-1101-2011

Song, F., Zhou, T., & Qian, Y. (2014). Responses of East Asian summer monsoon to natural and anthropogenic forcings in the 17 latest CMIP5 models. *Geophys. Res. Lett.*, *41*(2), 596–603. doi: https://doi.org/10.1002/2013gl058705

Stahle, D. W., Cook, E. R., Diaz, J. V., Fye, F. K., Burnette, D. J., Griffin, D., ... Heim Jr, R. R. (2009). Early 21st-century drought in mexico. *Eos Trans. AGU*, *90*(11), 89–90. doi: https://doi.org/10.1029/2009eo110001

Stevens, B., & Feingold, G. (2009). Untangling aerosol effects on clouds and precipitation in a buffered system. *Nature*, *461*(7264), 607–613. doi: https://doi.org/10.1038/nature08281

Stocker, T. F., Qin, D., Plattner, G.-K., Tignor, M., Allen, S. K., Boschung, J., ... others (2013). *Climate change 2013: The physical science basis*. Cambridge University Press Cambridge.

Taylor, M. A., Stephenson, T. S., Chen, A. A., & Stephenson, K. A. (2012). Climate change and the Caribbean: review and response. *Caribb. Stud.*, 169–200. doi: https://doi.org/

10.1353/crb.2012.0020

Ting, M. (1994). Maintenance of northern summer stationary waves in a GCM. *J. Atmos. Sci.*, *51*(22), 3286–3308.

Twomey, S. (1977). The influence of pollution on the shortwave albedo of clouds. *J. Atmos. Sci.*, *34*(7), 1149–1152. doi: https://doi.org/10.1175/1520-0469(1977)034⟨1149:tiopot⟩2.0.co;2

Undorf, S. (2019). Isolating the impact of North American and European anthropogenic aerosol emissions since the early instrumental period. *The University of Edinburgh*.

Undorf, S., Bollasina, M., Booth, B., & Hegerl, G. (2018). Contrasting the effects of the 1850–1975 increase in sulphate aerosols from North America and Europe on the Atlantic in the CESM. *Geophys. Res. Lett.*, *45*(21), 11–930. doi: https://doi.org/10.1029/2018GL079970

Undorf, S., Polson, D., Bollasina, M., Ming, Y., Schurer, A., & Hegerl, G. (2018). Detectable impact of local and remote anthropogenic aerosols on the 20th century changes of West African and South Asian monsoon precipitation. *J. Geophys. Res. Atmos.*, *123*(10), 4871–4889. doi: https://doi.org/10.1029/2017jd027711

Vega-Camarena, J. P., Brito-Castillo, L., Farfán, L. M., Gochis, D. J., Pineda-Martínez, L. F., & Díaz, S. C. (2018). Ocean–atmosphere conditions related to severe and persistent droughts in the mexican altiplano. *Int. J. Climatol.*, *38*(2), 853–866.

Wang, H., Schubert, S., Suarez, M., Chen, J., Hoerling, M., Kumar, A., & Pegion, P. (2009). Attribution of the seasonality and regionality in climate trends over the United States during 1950–2000. *J. Clim.*, *22*(10), 2571–2590. doi: https://doi.org/10.1175/2008jcli2359.1

Weaver, S. J., & Nigam, S. (2008). Variability of the Great Plains low-level jet: Large-scale circulation context and hydroclimate impacts. *J. Clim.*, *21*(7), 1532–1551. doi: https://doi.org/10.1175/2007JCLI1586.1

Weaver, S. J., & Nigam, S. (2011). Recurrent supersynoptic evolution of the Great Plains low-level jet. *J. Clim.*, *24*(2), 575–582. doi: https://doi.org/10.1175/2010JCLI3445.1

Westervelt, D., Conley, A., Fiore, A., Lamarque, J., Shindell, D., Previdi, M., ... Horowitz, L. (2018). Connecting regional aerosol emissions reductions to local and remote precipitation responses. *Atmos. Chem. Phys.*, *18*(16), 12461–12475. doi: https://doi.org/10.5194/acp-18-12461-2018

Westervelt, D., Conley, A., Fiore, A., Lamarque, J.-F., Shindell, D., Previdi, M., ... Horowitz, L. (2017). Multimodel precipitation responses to removal of US sulfur dioxide emissions. *J. Geophys. Res. Atmos.*, *122*(9), 5024–5038. doi: https://doi.org/10.1002/2017jd026756

Westervelt, D., Horowitz, L., Naik, V., & Mauzerall, D. L. (2015). Radiative forcing and climate response to projected 21st century aerosol decreases. *Atmos. Chem. Phys. Discuss.*, *15*(6). doi: https://doi.org/10.5194/acp-15-12681-2015

Wilcox, L. J., Dunstone, N., Lewinschal, A., Bollasina, M., Ekman, A. M., & Highwood, E. J. (2019). Mechanisms for a remote response to asian aerosol emissions in boreal winter. *Atmos Chem. Phys.*, *19*, 9081–9095. doi: https://doi.org/10.5194/acp-19-9081-2019

Wuebbles, D. J., Fahey, D. W., & Hibbard, K. A. (2017). Climate science special report: fourth national climate assessment. , *I*. doi: 10.7930/J08S4N35

Yu, S., Alapaty, K., Mathur, R., Pleim, J., Zhang, Y., Nolte, C., ... Nagashima, T. (2014). Attribution of the United States "warming hole": Aerosol indirect effect and precipitable water vapor. *Sci. Rep.*, *4*, 6929. doi: https://doi.org/10.1038/srep06929

Zelinka, M. D., Andrews, T., Forster, P. M., & Taylor, K. E. (2014). Quantifying components of aerosol-cloud-radiation interactions in climate models. *J. Geophys. Res. Atmos.*, *119*(12), 7599–7615. doi: https://doi.org/10.1002/2014JD021710